# Side Polished Fiber: A Versatile Platform for Compact Fiber Devices and Sensors

Linqing ZHUO[1], Jieyuan TANG[2], Wenguo ZHU[3], Huadan ZHENG[2], Heyuan GUAN[1,2], Huihui LU[1,3], Yaofei CHEN[2,3], Yunhan LUO[1,2], Jun ZHANG[1], Yongchun ZHONG[3], Jianhui YU[1], and Zhe CHEN[2,3*]

[1]*Key Laboratory of Optoelectronic Information and Sensing Technologies of Guangdong Higher Education Institutes, Department of Optoelectronic Engineering, Jinan University, Guangzhou 510632, China*

[2]*Engineering Research Center on Visible Light Communication of Guangdong Province, Department of Optoelectronic Engineering, Jinan University, Guangzhou 510632, China*

[3]*Key Laboratory of Visible Light Communications of Guangzhou, Jinan University, Guangzhou 510632, China*

[*]Corresponding author: Zhe CHEN E-mail: thzhechen@jnu.edu.cn

**Abstract:** Side polished fiber (SPF) has a controllable average roughness and length of the side-polishing region, which becomes a versatile platform for integrating multiple materials to interact with the evanescent field to fabricate all-fiber devices and sensors. It has been widely used in couplers, filters, polarizers, optical attenuators, photodetectors, modulators, and sensors for temperature, humidity, strain, biological molecules, chemical gas, and vector magnetic monitoring. In this article, an overview of the development history, fabrication techniques, fiber types, transmission characteristics, and varied recent applications of SPFs are reviewed. Firstly, the fabrication techniques of SPFs are reviewed, including the V-groove assisted polishing technique and wheel polishing technique. Then, the different types of SPFs and their characteristics are discussed. Finally, various applications of SPFs are discussed and concluded theoretically and experimentally, including their principles and structures. When designing the device, the residual thickness and polishing lengths of the SPF need to be appropriately selected in order to obtain the best performance. Developing all-fiber devices and sensors is aimed at practical usability under harsh environments and allows to avoid the high coupling loss between optical fibers and on-chip integrated devices.

**Keywords:** Side polished fiber (SPF); V-groove assisted polishing technique; wheel polishing technique; lab-on-fiber; fiber devices; sensors

Citation: Linqing ZHUO, Jieyuan TANG, Wenguo ZHU, Huadan ZHENG, Heyuan GUAN, Huihui LU, *et al.*, "Side Polished Fiber: A Versatile Platform for Compact Fiber Devices and Sensors," *Photonic Sensors*, 2023, 13(1): 230120.

## 1. Introduction

In high-performance integrated circuits, on-chip optical interconnects have the potential for solving the communication bottleneck. At present, on-chip optical interconnects mainly rely on silicon photonics [1, 2]. However, the precise coupling between the silicon waveguide and the optical fiber mainly through optical gratings or taper fibers usually requires the long assembly time and cost [3]. Moreover, combining with the few-mode fiber and multi-core fiber is a challenge, and the grating coupling has limited the bandwidth. The development of the optical fiber versatile platform

Received: 7 November 2021 / Revised: 3 April 2022

DOI: 10.1007/s13320-022-0661-x
Article type: Review

meets the requirements of all-fiber integration and expects to achieve seamless connection between optoelectronic devices and optic fiber networks. The concept of "lab-on-fiber" has attracted a great attention since 2012, which is a new technology that integrates highly functionalized micro/nano-structures and materials on optical fibers [4–6]. This technology helps to realize a small and compact optical fiber system and develop the all-in-fiber device. It will allow the "lab" to be combined with transmission mechanisms and integrated into modern optical systems for communication and sensing applications [4]. In addition, the lab-on-fiber has the advantages of resisting electromagnetic interference, small size, geometric versatility, and compatibility with fiber optic systems.

In the past few decades, the emergence of the optical fiber has promoted the development of the communication field, which becomes an important optical waveguide. Therefore, optical fiber-based optoelectronic devices and sensors emerged at the historic moment [7–11]. With the maturity of the microfabrication technology and the emergence of two-dimensional (2D) materials, the foundation has been laid for the fabrication and integration of the nanostructure on optic fibers. Since Bergh *et al*. [12] polished the first side polished fiber (SPF) in 1980, the research on SPFs has a history of 40 years. By removing part of the fiber cladding, the cross section of the polished area looks like a D-shape and the unpolished fiber section is still cylindrical. The side-polishing region of SPFs provides a flat platform for the integration of the micro-and nanostructures to realize effective light-matter interaction [13]. Hence, SPFs can be a versatile platform for optical fiber compactable devices and sensors.

This paper reviews the fabrication techniques, characteristics, fiber types, and applications of SPFs. The article is organized as follows. Firstly, the fabrication techniques of SPFs are described, including the V-groove assisted polishing technique and wheel polishing technique. Then, different types of SPFs and their characteristics are explained in detail. Finally, various applications of SPFs are introduced in detail, including their principles and structures. The reliable mechanical properties and anti-electromagnetic interference properties make the SPF widely suitable for applications in fiber couplers, filters, polarizers, photodetectors, sensors, etc. The SPF has the advantages of direct compatibility with the theoptical fiber, low insertion loss (0.1 dB), minimized polarization-dependent loss (<0.02 dB), and wide operational bandwidth, which has attracted more interests in the construction of all-fiber devices or functional fiber sensors as a versatile platform.

## 2. Fabrication techniques of the side polished fiber

The development of the optical fiber side polishing technology has a history of 40 years. Some reliable polishing techniques of fabricating SPFs without introducing excessive loss and the method of non-destructively estimating the residual thickness have attracted a lot of attention. Generally, the manufacturing process of a standard SPF begins with a rough lapping process to remove the cladding and then a fine polishing process to remove the surface scratches. However, a high-quality SPF with the smooth polished surface usually takes a long side-polishing time. Researchers have continuously tried and improved the fabrication technology of the SPF, mainly including the V-groove assisted polishing technique and wheel polishing technique. Before side-polishing, the complete fiber cladding ensures that the optical wave will be transmitted in the core. When part of the cladding of the fiber is removed, a portion of the optical signal leaks through the fiber core and into the cladding through an evanescent field that decays exponentially with the distance from the polished surface to the core.

### 2.1 V-groove assisted polishing technique

One of the reliable polishing techniques of producing an SPF is the V-groove assisted polishing technique. This technique requires supporting grooves or blocks to support the optical fiber, and the fiber will grind or polish simultaneously with the block substrate, as shown in Fig. 1(a). Tseng *et al*. [13] first reported a reproducible silicon V-groove assisted polishing technique and estimated the polishing depth by the liquid-drop method. Pei *et al*. [14] used the arc discharge method to improve the roughness of the polished surface and suppress the large loss caused by microcracks or pits, and they independently developed an equipment to precisely control the polishing depth of the SPFs. Dikovska *et al*. [15] engraved multiple V-grooves on an oxyfluoride glass, which can achieve simultaneous polishing of multiple optical fibers and greatly improve the efficiency. It usually takes several polishing steps to obtain a standard SPF. Firstly, coarse abrasive powders are used to polish one or more times, and then a few micrometers particles are used to finely polish. The disadvantage of this method is that a groove must be engraved on the substrate first, and each fiber needs a newly engraved groove substrate. In addition, the optical fiber should be fixed with epoxy glue, and after polishing, chemical solvents need to be used to dissolve the epoxy glue. This technique is costly, time-consuming, environmentally unfriendly, and difficult in mass production. What's more, the SPF made by this method is difficult to ensure the consistent polishing depth of the entire polishing region and difficult to make a long side-polishing region [16].

### 2.2 Wheel polishing technique

Another method to produce an SPF without blocks is the wheel polishing technique [17, 18], which is suitable for various types of fiber, including the single-mode fiber (SMF-28e), few-mode fiber, multimode fiber, panda fiber, and plastic optical fiber [19–22]. It has the advantages of simple operation, low cost, and no need to use glue to fix, and the middle of the side-polishing region is completely flat. This technique also allows to polish multiple optical fibers at the same time. The optical fiber with a section of the coating stripped is suspended tightly above the fixed motor-driven wheel by two fiber clampers and then dropped paroline oil onto the abrasive paper as lubrication. By adjusting the size of the polishing wheel to control the length of the polishing region, the polishing depth is estimated by in situ monitoring the optical power online [23, 24]. Connecting the light source and optical power meter to both ends of the fiber, by observing the throughput attenuation during the light propagation, can monitor the whole polishing process. The abrasive paper is wrapped around the wheel by the double-sided tape to uniform polishing. The wheel can be driven by a low-cost 6 V direct current (DC) motor, and the stress and the speed of the wheel can be turned [24]. The length of the side-polishing region can be controlled from 2 mm to 60 mm [17]. The manufacture of the SPF starts with the rough lapping process of the coarse abrasive paper, which makes the remaining thickness of the SPF drop rapidly and then starts a fine polishing process to remove scratches on the polishing surface. The roughness of the polishing region is determined by the polishing time and the grit size of the abrasive paper. Zhao *et al*. [25] demonstrated a fast mechanical wheel lapping technique to fabricate a rough SPF, the surface scratches are discontinuous and malposed as observed by 5000×SEM, and the schematic diagram of the wheel polishing setup and the surface scratches of the SPF is shown in Fig. 1(b). These scratches will cause a large insertion loss (10 dB ~ 30 dB) by surface scattering. Jinan University has independently developed a fully automated wheel side polishing equipment with a microscopic imaging system [as shown in Fig. 1(c)]. The commercial mass production of the SPF has been achieved. It is equipped with multiple laser sources

and power meters for online monitoring [26], which realizes the control of length, depth, angle, shape, and roughness of the side-polishing region and the fiber tension. By precise control and a fine polishing process by the 15000-mesh abrasive paper, the side-polishing region of the single mode SPF polished by Jinan University is smooth. The average roughness is smaller than 22 nm according to the atomic force microscopy (AFM) image of the side-polishing region, and the test range is 25 μm$^2$, as shown in Fig. 1(c).

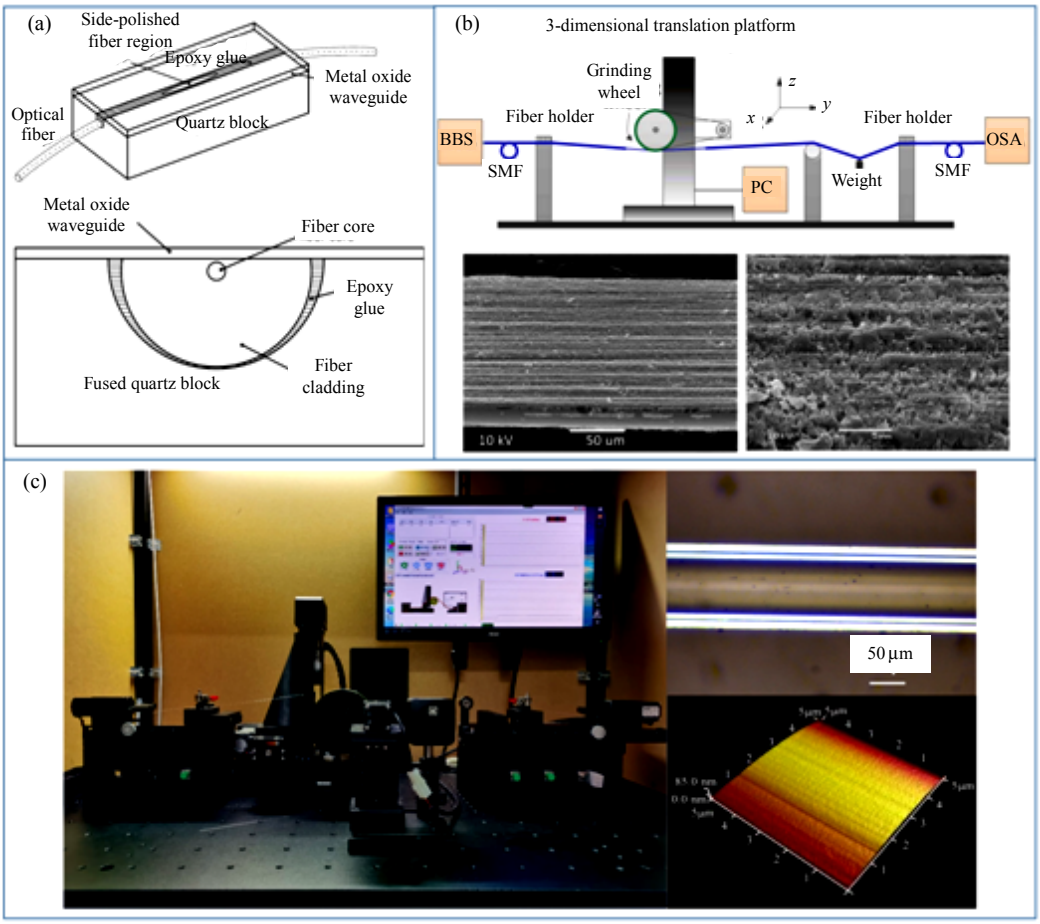


Fig. 1 Schematic diagram of the V-groove assisted polishing technique (a) [15], wheel polishing technique (b) [25], and fully automated wheel side polishing equipment, microscope picture of the side-polishing region of single mode SPF, and its AFM image polished by Jinan University (c). BBS: broadband light source; OSA: optical spectrum analyzer; PC: personal computer.

## 3. Various types of polished fiber and their characteristics

The SPF consists of three parts: the lead-in and lead-out optical fiber, the transitional region, and the flat region, as shown in Fig. 2(a). Before side polishing, the whole cladding ensures that the optical wave will be transmitted in the fiber core, and the evanescent field in the cladding does not leak out of the fiber. When polishing away part of the cladding to fabricate an SPF, the distance between the polished surface and the core is only a few microns, so the evanescent field will leak from the polished region [27]. The flat region is in the middle of the polished region, and the two sides of the flat region are the transition regions. The residual thickness (RT) is defined as the distance from the polished surface to the fiber bottom surface,

which determines the strength of interaction of the transmission light in the SPF with the external media [13].

For the wheel polishing technique, the transition region is an arc-shaped area with a gradual cladding thickness whose radius of the curvature depends on the diameter of the wheel. The transitional region provides an efficient way to excite the high-order modes and strong evanescent field of the SPF [28]. There are many methods for measuring the RT, including the use of mechanical comparators, measuring the length of the oval polished section of the fiber [29], the liquid-drop method [29], and in-situ monitoring technique [23]. Among them, the in-situ monitoring technique has the advantage of high efficiency, precision, reproducibility within 1 μm, and no need for refractive index matching fluid [23].

### 3.1 Single-mode fiber and multi-mode fiber

The SMF and multi-mode fiber (MMF) are the most two common optical fiber types in SPFs. Because of their low cost and easy polishing characteristics, they have been widely used in the sensing field and optical fiber communications. By polishing a part of the cladding of the SMF or MMF, the evanescent field can easily leak from the fiber core.

The transmission spectrum of the side-polished SMF is related to the RT, and the transmission spectrum of the original SMF shows nearly none power loss, as shown in Fig. 2(b). As the RT decreases continually, the power loss gradually increases until the RT reaches 71 μm. When polishing close to the fiber core (RT<69 μm), the peaks/dips in the transmitted spectrum can be observed owing to the multimode interference [30], and the extinction ratio of the interference spectrum reaches 5 dB when RT = 68.1 μm [25]. When the RT of the SPF keeps unchanged, increasing the polishing length will increase the loss, as shown in Fig. 2(c) [25]. In addition, there are some studies on the transmitted optical power through the SPF changed with the surrounding refractive index [27, 31, 32]. The external medium can be an effective mode sink when polished close to the fiber core. As shown in Fig. 2(d), when overlaying the oil with different refractive index ($n_{oil}$) values on the polished region, the optical power loss is less than 1 dB under the condition of $n_{oil}$ <1.4378, the optical power loss swiftly increases from 1 dB to 60 dB (1 310 nm) when $n_{oil}$ increases from 1.437 8 to 1.452 1, and the loss of optical power decreases gradually and levels off at a certain value when $n_{oil}$ > 1.453 2 [27]. The result shows that the loss of optical power at 1310 nm is larger than that at 1550 nm.

Figures 2(e) – 2(g) show some simulation results, including the theoretical calculation of the optical power loss of the side-polished SMF changed with the refractive index of the overlaying material [32], transmission spectra, and field evolution of the coreless side-polished fiber (CSPF) by the commercial beam propagation method (BPM) module from Rsoft Inc [28]. The simulation results show that some dips/peaks exist in the transmission spectra and the spectra have a red shift when the surrounding refractive index increases from 1.454 to 1.456, as shown in Fig. 2(f). The light enters the SPF in the form of the fundamental mode by the lead-in SMF and is reflected in the polished region to excite the high-order modes. This phenomenon is called the multimode interference (MMI) which will result in interference peaks/dips in transmission spectra due to the constructive/destructive interference. Xiao *et al*. [33] calculated numerically the effective mode index (EMI) of a graphene-coated SPF modulator. The simulation result shows that the field distribution is related to the residual thickness of the SPF, as shown in Fig. 2(g). With a decrease in the residual thickness, the mode field distribution moves from the fiber core to the cladding which is gradually far from the graphene. This modulator is theoretically predicted to have a 0.007 2 dB/μm modulation depth and 56.2 THz optical modulation

bandwidth [33].

The side-polished MMF can excite much higher order modes than the unpolished MMF. Multiple modes cause MMI and result in an increased number of speckles in the transverse light field [34]. It has been verified that the number of the excited modes is proportional to the number of speckles in side-polished MMF output specklegrams [35]. Hence, the side-polished MMF will increase the sensitivity of light guidance in the optical fiber to changes in the surrounding environment. Mu *et al*. [35] verified that the excited modes are more sensitive to the surroundings at larger side-polishing depth and length. Yang *et al*. [36] compared the performance of the hydrogen sensor based on the side-polished SMF and MMF, and found that the MMF-based sensor showed much greater change of transmitted power. Figures 2(h) – 2(k) are the cross-section pictures of different types of SPFs polished by the team of Jinan University, including the side-polished SMF, MMF, polarization maintaining panda fiber, and photonic crystal fibers (PCF).

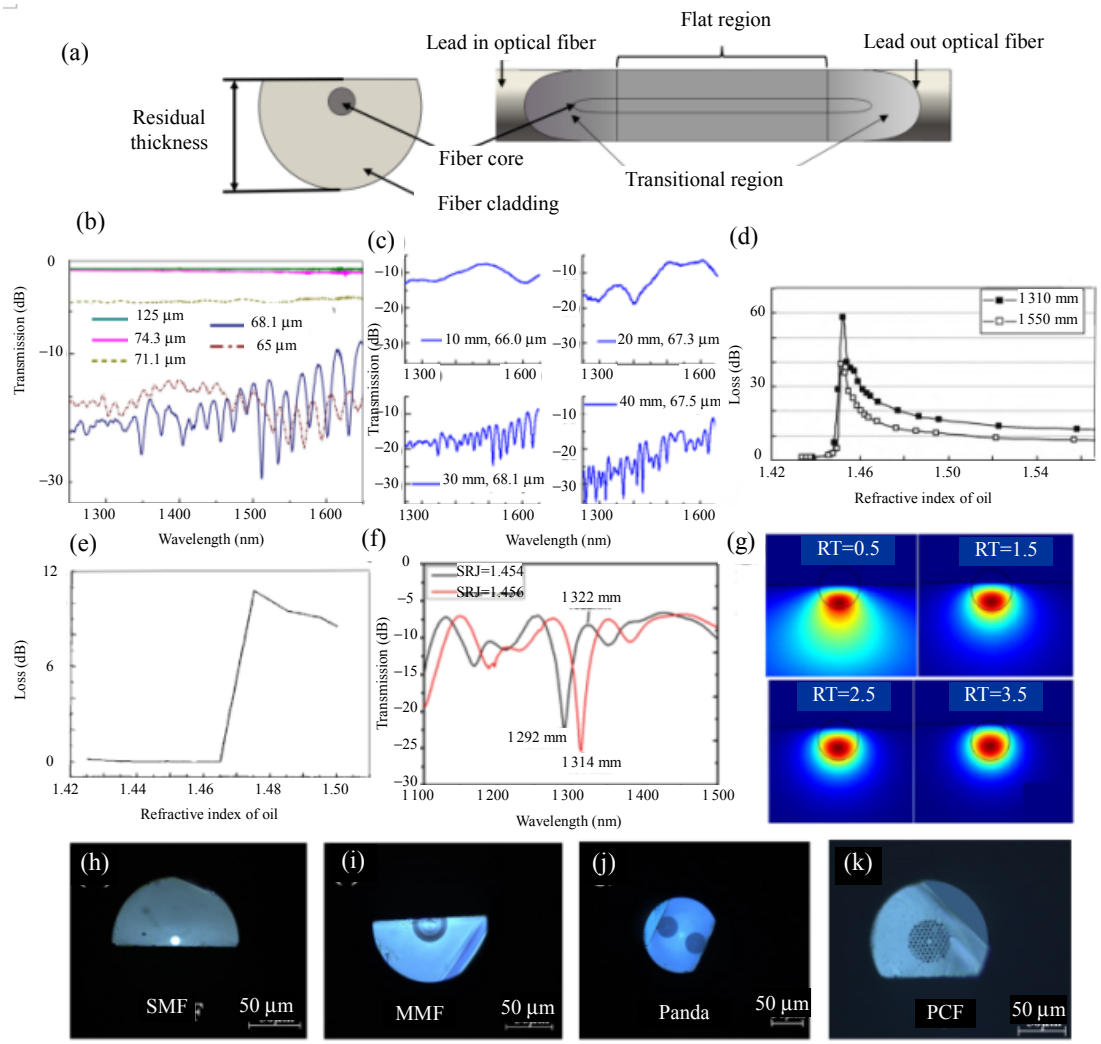


Fig. 2 Characteristics of the SPF: (a) cross section of the polished area and top view of the SPF, (b) transmission spectrum evolution of the SPF with the 30 mm polishing length, the residual thickness reduces from 125 μm to 65 μm [25], (c) transmission spectrums of different polishing lengths (10 mm, 20 mm, 30 mm, and 40 mm) of four SPFs with similar residual thickness [25], (d) loss of transmission optical power in the SPF varies with the refractive index of the overlaying material [27], (e) theoretical calculation of the optical power loss changed with the refractive index of the overlaying material [32], (f) transmission spectra of the CSPF with an RT of 53.3 μm, (g) the simulated result of field distribution of TE-mode changing with RT [28], and (h) – (k) the cross-section pictures of different types of SPFs polished by Jinan University.

### 3.2 Polarization maintaining fiber

The polarization maintaining fiber (PMF) is popular for its unique characteristics of two orthogonal polarization modes, which can propagate at different phase velocities [20, 37]. According to the difference in the shape of the stress zone, the PMF can be divided into the panda fiber, bow-tie fiber, and ellipse fiber. The polishing PMF is more complicated than the polishing SMF, and it needs to measure the polarization stress axis of the PMF first. The side polishing of the PMF is along the slow or fast axis. Only when the polarization can be maintained on the entire fiber system, the polarization maintaining properties of side polished PMFs can be fully exploited. Until now, the azimuthal alignment method for the PMF without the coating includes the polarization observation by the lens-effect-tracing (POL) method [38–40], direct monitoring method using the central image [41], five-point eigenvalue method [42], light intensity distributions eigenvalue method with the five-finger profile [43], and ray-tracing method [44]. The principle of the POL method is based on the anisotropy of the lens effect of the PMF. The POL method setup usually consists of the fiber optic lamp, mirror, fiber rotator, objective lens, charge coupled device (CCD) camera, and monitor. A successful side-polished PMF still possesses the birefringence, and the polarization dependent loss (PDL) measured by the liquid-drop method is negligible [45]. Base on the POL method, Wang *et al*. [39] proposed a new polarization observation by lens-effect-tracing with the middle-line (POLM) method to improve the precision of angle orientation within 1°. Zhen *et al*. [46] established an on-line setup of the azimuthal position observation by the POL method which realized on-line adjusting axes of the PMF with and without the coating. The side-polished PMFs have been successfully used in asymmetric directional couplers, strain measurement, and optical sensors [47, 48]. King *et al*. [20] used the side-polished panda fiber to fabricate an electric field sensor by the slab-coupled optical sensor technology. Wu *et al*. [48] first reported Sagnac interferometers for the strain measurement and surface plasmon resonance (SPR) biochemical sensing using two types of side-polished panda fibers. These works indicated that side-polished panda fibers could manufacture promising optical fiber devices for the Internet of things sensing technology.

### 3.3 Micro-structure fibers

The PCF is also called micro-structure fiber, which usually includes the hollow core PCF and solid core PCF, which has endless single mode transmission, high birefringence, and high nonlinearity optical characteristics [49]. In general, the PCF is composed of periodic refractive index distribution in the cladding and/or core. The unique properties make the PCF show better sensing performance than conventional fibers, especially the side-polished PCF has been successfully applied to bio-sensing, refractive index sensing, SPR sensing, and optic coupler [50–53]. Le *et al*. [53] designed a symmetrical side-polished PCF structure to solve the problem of temperature cross-sensitivity of the magnetic field sensor by commercial finite element software Comsol Multiphysics. He *et al*. [54] analyzed optical propagation characteristics of the side-polished PCF with the residual thickness, polished length along the PCF, and azimuth by use of the 3D finite difference beam propagation method. This article shows the optical power transmittance of the side-polished PCF decreases and oscillates as the polishing length increases and residual thickness decreases. When the innermost layer of air holes of the PCF has been side polished, the fundamental mode field is mainly constrained in the central solid area even though the symmetric periodical configuration of the PCF has been destructed. What's more, in the polished area, the originally launched fundamental mode will be coupled to the high order propagation modes and radiation mode [54].

### 3.4 Bragg fibers

Bragg fibers (BFs) are a kind of photonic bandgap fibers proposed in 1978 which has unique dispersion and modal properties [55, 56]. BFs can be classified into hollow-core-BFs and solid-core-BFs, which have an alternating cladding of high and low refractive indices. Due to the easy control band gap, BFs can be used as wavelength-dependent distributed filters [56]. Among them, the potential application of hollow-core-BFs is the low loss of $CO_2$ laser transmission and trace gas sensing in the mid-infrared region [57]. The basic principle of BGs sensing devices is to monitor the wavelength shift of the reflective signal for any changes in the external physical parameters. The side-polished BGs increase the sensitivity of fiber sensors because of a decrease in the distance from the external to the core, and the reflection and transmission spectra can be observed by an OSA. Another optical fiber with periodically changes of core refractive index is the fiber Bragg grating (FBG). By monitor the wavelength shift of the returned Bragg signal to measure the change of the environment parameter, side-polished FBGs have been widely used in hydrogen sensors, magnetic sensors, and refractive index sensors [58–60].

### 3.5 Plastic fibers

Plastic fibers (PFs) are also called polymer optical fibers. The first plastic fiber was produced at the end of the 1960s by DuPont, and PFs have the advantages of physical robustness and can operate in the visible light regime [61]. Generally, PFs have a large fiber core with diameters of 0.25 mm – 1 mm which allows to use the lower precision connectors in the optical system to reduce the cost [62]. Some polymers like poly (methyl methacrylate) (PMMA) are the most commonly used to produce PFs, and they have the characteristic of resistance to impacts and vibrations, and large elastic deformation limits (10%) [62, 63]. Compared with the silica fiber, the materials of PFs are softer which makes the side-polishing procedure simpler. Although PFs have been successfully applied to curvature and refractive index sensors [22, 61], the large attenuation about 125 dB/km (650 nm) has restricted its long-range application.

### 3.6 Multi-core fibers

Multi-core fibers have been considered as a promising way to increase the capacity of communication systems. An effective way to increase the number of cores in a multi-core fiber is by enlarging the cladding diameter and relaxing the requirement for inter-core crosstalk [64]. By the side-polishing approach, we can choose to interact with a core in the multi-core fiber without introducing large additional losses. Side-polished multi-core fibers have become an important platform for the directional coupler [64], phase modulator [65, 66], and directional coupler-based relative humidity sensor [67]. Especially, the side-polished twin-core fiber is widely used, and the side-polished core and unpolished core act independently as two arms of the Michelson interferometer, which can realize phase modulation [64, 65].

## 4. Applications of the side polished fiber

In all-fiber devices and sensors, it is necessary to realize light-matter interaction via an evanescent field. When a part of the cladding has been removed, the SPF offers the evanescent field to allow interaction between the light and the external environment, which makes it an ideal miniaturized platform for exploring optical fiber couplers [49, 68–73], filters [74–79], resonators [80–84], polarizers [85–93], attenuators [94–96], state of polarization controllers [97–100], optoelectronic devices [10, 11, 33, 101–107], and optical sensors [108–147].

### 4.1 Optical fiber devices

#### 4.1.1 Couplers

Optical fiber couplers are key passive components to realize the light of different channels

bonding or splitting in the optical communication system [49]. The coupling ratio, excess loss, and insertion loss are important parameters to characterize fiber optic couplers [68]. The couplers can be made of the SMF, MMF, PMF, and PCF. Among them, the SMF optic coupler is most widely used in optical communications, sensing, and fiber lasers. One of the methods to fabricate fiber couplers is the fused biconical taper method [69], while this method is not suitable for the fabrication of PCF couplers, which will destroy the internal structure of the PCF and induce defects. During the fusing process, the air hole will suffer from collapse and the cladding layer will distort [49]. Another fabrication method is based on the side-polishing technique. Zhang *et al*. [70] proposed a broadband mode-selective coupler by a side-polished six mode fiber and a tapered side-polished single-mode fiber, and they observed that the coupling ratios were larger than 85%, as shown in Fig. 3(a). Kim *et al*. [71] fabricated a coupler with a tunable coupling ratio by controlling the parameters of two side-polished PCFs [71]. For PCFs couplers, the side-polishing technique has the following advantages: the coupling efficiency can be easily adjusted by controlling the matching parameters and the pore structure of PCFs will not be deformed. Luo *et al*. [72] purposed a novel side-adhering technique to fabricate the fiber coupler, which was validated by the fabrication of the side-polished SMF coupler. Some nano silica powders were deposited at the flat polished area, and when encountering oxy-hydrogen flame, the nano silica powders would melt and adhere two side-polished fibers. Zhu *et al*. [49] fabricated a PCF coupler by the side-adhering technique, and they got the best fabrication parameters (polishing angle = 0°, residual radius = 5.7 μm) by the theoretical analysis. If the polishing angle and residual radius are not properly selected during the fabrication process, it may result in a significant loss of the side-adhered PCF coupler [73]. This technique orders a direction for further research and development of the side-polished PCF coupler and commercial PCF coupler.

#### 4.1.2 Filters

The optical fiber filter is one of the key components in the wavelength division multiplexing (WDM) optical communication system and sensing system. It is developing towards the tunable wavelength and low insertion loss. The common structural designs of the filters are based on the coupler, fiber grating, fiber interferometers, etc. [74–76]. Each type of fiber filters has its own filtering and tunable range. In 1994, Archambault *et al*. [77] used a 2×2 side-polished SMF grating-frustrated coupler to form a low-loss (0.22 dB) channel-dropping filter, which exhibited the 0.7 nm bandwidth and 13 dB isolation, and one of the side-polished SMF cores contained an index grating. Near the Bragg wavelength, the filter would not operate as a conventional coupler, and the grating would frustrate the transfer of the optical power from Fiber 1 to Fiber 2 [77]. Lausten *et al*. [78] demonstrated an arbitrarily tunable and optically reconfigurable Bragg filter by azopolymer-coated SPF blocks, which could realize the optically write-erase-write cycle. Yu *et al*. [76] proposed an all-optically reconfigurable and tunable band-rejection filter by overlaying the photosensitive liquid crystals (P-LCs) hybrid film on the SPF, as shown in Fig. 3(b). This filter showed a wider tunable bandwidth of 60 nm, and the extinction ratio was as high as 21.5 dB and 23.4 dB when the P-LCs were reconfigured as short-period and long-period fiber surface gratings, respectively. P-LCs had a large and tunable birefringence characteristic that allowed to construct optically tunable and reconfigurable photonic device by an external field [76]. Yu *et al*. [79] also reported a wavelength dependent optical fiber add-drop filter based on a micro/nano fiber ring and an SPF, when the micro/nano fiber ring diameter was 580 mm, the add-drop filter reached the maximum extinction ratio

of the drop port and the add port were 7.5 dB and 4.8 dB, respectively. The SPF serves as an integrated platform and provides an evanescent field to interact with the guided light mode filed to realize in-line light coupling and can seamlessly connect with a conventional optical fiber system.

#### 4.1.3 Optical resonators

Optical resonators have been explored for many optical applications such as wavelength-selective reflectors and filters, switches, spectrum analyzers, and nonlinear optical devices [80–82]. Fabricating resonators on the optical fiber promises to avoid coupling loss, reliability, and cost issues of fiber-to-chip coupling [83]. Compared with the curved plane of an unpolished fiber, the SPF has a flat side-polishing region, making it easier to fabricate micro-structures on this flat region. And the SPF substrate allows the resonators to be easily connected to fiber systems and other fiber resonators. Sherwood *et al*. [83] used the two-photon polymerization to fabricate polymer ring resonators on an SPF, and the rough surface limited the *Q*-factor in the range of 300 – 400. About ten years later, Shi *et al*. [81–84] fabricated whispering gallery mode (WGM) resonators on the SPF by femtosecond laser micromachining. By femtosecond laser ablation, they fabricated the cylindrical resonator cavity in the SPF to achieve a WGM resonator [in Fig. 3(c)] with a *Q*-factor of $1.44\times10^3$ at 1556.52 nm [82]. It is more time-efficiency to machine the micro-structure on the SPF, because the debris accumulated on the SPF is much less than that in the unpolished fiber during the femtosecond laser ablation process. However, restricted by the average surface roughness after femtosecond laser ablation, the maximum *Q*-factor is limited to $10^3$, which is smaller than those of the tapered fiber coupled WGM resonators.

#### 4.1.4 Polarizers

The fiber-optic polarizer is one of the essential components in both optical communications systems and polarization-dependent sensing systems for selecting the polarization of electromagnetic waves. The asymmetric structure of the SPF produces a large attenuation difference between orthogonal polarizations modes, thus becoming a favorable platform for the preparation of polarizers. Many kinds of overlays, such as birefringent polymer thin films [85], metal films [86], birefringent crystals [87], and optical phase change materials [88], have been used to make in-line SPF polarizers. These overlays have only one guided polarization state, while the other polarization state is not supported and will be absorbed or radiated. With the appearance of 2D materials, some SPF-based graphene polarizers with a high extinction ratio have become promising candidates, because graphene can use the linear dispersion of Dirac electrons to select TE or TM surface plasmon mode to support, as shown in Fig. 3(d) [89–91]. Table 1 presents an overview of the SPF polarizers with different overlay materials, including the implementation and performance of each study [85–89, 92]. From the comparison result, the SPF polarizers show a low insertion loss, but researchers need to enhance the light-matter interaction to further improve the extinction ratio. Although the extinction ratio of the fiber-optic polarizer is smaller than that of the birefringent crystals polarizer (~$10^4$:1) [93], it is simpler, smaller, and with a less loss in connection to optical fiber systems.

Table 1 Comparison of the SPF polarizers with different overlay materials.

| Materials | Extinction ratio (dB) | Insertion loss (dB) | Reference |
|---|---|---|---|
| Polymer polyvinyl carbazole | 36 | 0.5 | [85] |
| Thin-metal-film | 33.1 | 1.1 | [86] |
| Birefringent crystal | 60 | – | [87] |
| PMMA/graphene/$VO_2$/graphene | 164 | 3.86 | [88] |
| Graphene | 27 | 5 | [89] |
| $MoS_2$/graphene/Au | 19.2 | – | [92] |

#### 4.1.5 Attenuators

Fiber-optic attenuators can regulate the optical power propagated in fiber optical communication and WDM networks. In fiber optical communication networks, the variable optical attenuators (VOAs) are used to dynamically control the optical power from light sources and optimize the optoelectronic responses of high-speed receivers to avoid overload [94–96]. With the development of communication networks, the pursuit of the low-cost and high-performance VOA has become the focus of research. All-fiber devices provide an excellent technical solution for this need. The ideal VOA attenuation range is at least 20 dB optical attenuation, 40 nm optical operation bandwidth, and 1 dB wavelength dependent loss [94]. Commercial active VOAs are typically based on severing step index guiding fiber with a thin-film absorption filter on the cutting area [95]. The attenuation can be controlled dynamically by rotating or sliding the filter mechanically, so as to change the optical path length in the absorptive material. Compared with microelectro-mechanical systems (MEMS) optical fiber VOAs, the SPF-based optofluidic VOA used a single mode and continuous optical fiber [Fig. 3(e)] and achieved a broadband optical attenuation (40 nm bandwidth) with an optical attenuation range up to 26 dB, because it had not any fiber-gaps and fiber lenses between two fibers [94]. The first optically controllable P-LCs SPF attenuator operating at 1.5 μm has been demonstrated [95]. The attenuation was controlled by the photochemical-induced phase change of the P-LCs, which adjusted the evanescent field leaking from the side polishing area. When the environmental temperature was 45 ℃, this attenuator could reach a 15 dB optical attenuation with an optical field of 20 mW [95].

#### 4.1.6 State of polarization controllers

Controlling the state of polarization (SOP) is important to obtain desired performance characteristics, such as polarization conversion and power equalization in sensing and communication systems. So far, the manufacture of the all-fiber SOP controller is mainly based on two types of fibers: one is the PCF and the other is the SPF [97–100]. Both the PCF and the SPF SOP controllers have the advantages of high extinction ratio and low loss. As mentioned above, P-LCs have been successfully used for creating optically tunable SPF devices. Hsiao *et al*. [99] reported an optically tunable polarization rotator by covering P-LCs on the SPF as the overlaid birefringent material. Its working principle is to change the SOP of the propagated light and increase the phase shift by changing the power of the light irradiation. Except for the P-LCs, the chalcogenide glass film has also been coated onto the SPF to fabricate an optically switchable, inline, and all-fiber SOP controller [100]. An optically tunable SOP SPF controller based on the amorphous $As_2Se_3$ thin films has been demonstrated, as shown in Fig. 3(f). This SOP controller can achieve 70° phase retardation without the optical loss (<0.2 dB) [100].

#### 4.1.7 Optoelectronic devices

In recent years, all-fiber optoelectronic devices have been extensively studied due to the advantages of easy compatibility and high robustness. The SPF provides a flat platform for optoelectronic devices integration, and the excellent optical and electronic properties and flexibility of 2D materials makes “lab-on-fiber” possible. Recently, the 2D materials represented by graphene have been successfully integrated with the SPF to develop photodetectors, electro-optical modulators, optical phase modulators and fiber lasers [10, 11, 33, 101–103]. Among them, the most common applications are SPF-integrated graphene photodetectors and the optical modulators, which have been verified in both theory and experiment [10, 11, 33]. Zhuo *et al*. [11] assembled a hybrid carbon nanotubes (CNT)/graphene film onto the SPF to achieve an all-fiber integrated photodetector with an ultrahigh responsivity

of $1.48\times10^5$ A/W. The responsivity of the graphene-based photodetector has been greatly improved by CNTs because the CNT films exhibit an exceptional broad absorption from the ultraviolet to terahertz region [11, 104]. Except for the photodetectors, some SPF-based multifunctional graphene optoelectronic devices have been proposed as shown in Figs. 3(g) and 3(h). Assembling a hybrid graphene/polybutadiene (PB)/PMMA film on an SPF can achieve a high-performance fiber-integrated graphene-based device with dual functions: photodetection and optical phase modulation [91]. The light-graphene interaction has been enhanced by the extra-long side-polished region and the high refractive index of the PMMA, resulting in an ultra-high responsivity of $1.5\times10^7$ A/W at 1550 nm

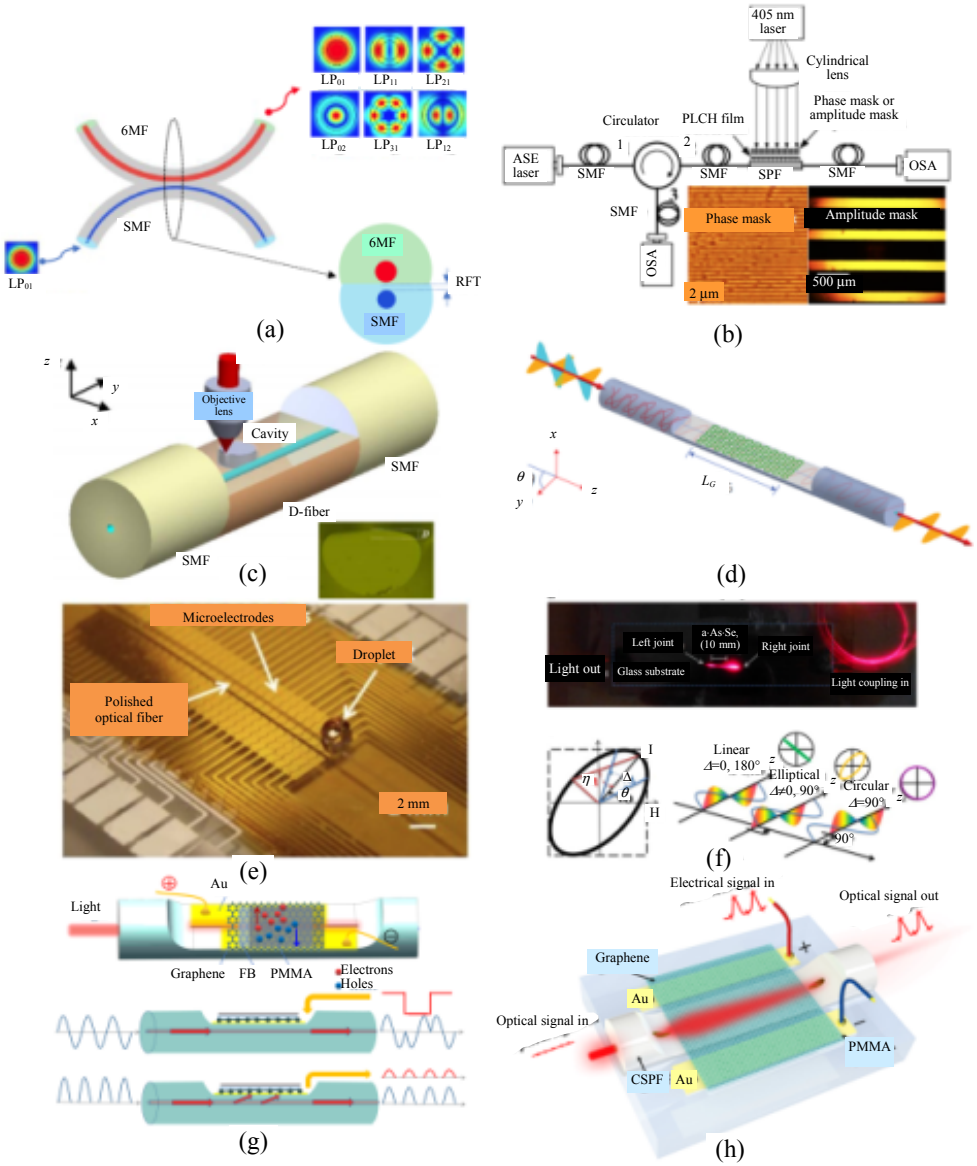


Fig. 3 SPF-based optical devices: (a) schematic diagram of a broadband mode-selective coupler [70], (b) schematic diagram of the experimental setup to test the performance of an optically tunable and reconfigurable SPF-based band-rejection filter [76], (c) schematic diagram of the whispering gallery mode (WGM) resonator [82], (d) schematic diagram of the graphene polarizer [89], (e) schematic diagram of the electrowetting-based single-mode SPF VOA platform [94], (f) schematic diagram of laser light coupling to SOP and the corresponding ellipticity of different SOP [100], (g) schematic diagram of the SPF-integrated graphene optic-phase modulator and photodetector [101], and (h) schematic diagram of the CSPF-integrated graphene electro-optical modulator and photodetector [10].

and a maximum phase shift of $3\pi$ [101]. A graphene/PMMA [Poly (methyl methacrylate)] hybrid film and CSPF-based device can work as both an electro-optical modulator with an amplitude modulation efficiency of 1.13 dB/V at a wavelength of 1540 nm, and a photodetector with a responsivity of 0.44 A/W in the near-infrared region [10]. SPF-integrated devices provide an in-line photodetection and modulation way to seamlessly connect with optical communication networks and provide a novel solution to break the ultra-weak interaction between light and 2D-materials [105–107]. Lee *et al*. [103] proposed an electric control of the all-fiber graphene device by using ion liquid as an efficient gating medium. By integrating this device into a fiber laser system, it can work as an electrically tunable in-line nonlinear saturable absorber and control the fiber laser operating at different regimes: continuous wave, *Q*-switching, and passive mode-locking [103]. This all-fiber electrically tunable device opens a hopeful way for actively controlling optoelectronic and nonlinear photonic devices in the SPF platform. These researches show that the SPF can be a reliable platform for realizing online multifunctional optoelectronic devices.

### 4.2 Various types of sensors

Since the 1970s, the development of fiber sensors is revolutionizing our life. Different from the electrochemical sensors, fiber sensors have the advantages of small size, remarkable compatibility, immunity to electromagnetic interference, and chemical inertness. Benefited from the flat polished surface and evanescent window of the SPF, more and more high-sensitive SPF-based sensors have been demonstrated [108–147]. A lot of studies have been carried out to combine the SPF with different optical materials to seek better sensors. The optical fiber sensors are prepared by coating sensitive materials on the side polished region of the SPF. When the external environment changes, the properties of the material will change, resulting in predictable changes in the optical power transmitted by the optical fiber.

#### 4.2.1 Refractive index sensors

Refractive index (RI) fiber sensors show a great value in biomedical, chemical, and food processing. To date, numerous RI fiber sensors have been reported, such as CSPF-based MMI RI sensors [28, 108], D-shaped PCF RI sensors based on the SPR [109–112], and MMI RI sensors based on the side polished single mode-multimode-single mode fiber (SP-SMSF) [19]. The SPR technique is pivotal to the field of optical sensors, and it is very sensitive to the refractive index of the surrounding environment with the help of the evanescent wave [111]. The SPR occurs at specific wavelengths, and the resonant wavelengths will shift when the environment changes slightly. Table 2 presents an overview of RI sensors, including the structure and performance of each study. From Table 2, the RI fiber sensor based on the SPR technique has the advantage of detecting tiny RI changes because the SPR is very sensitive to the change of the surrounding environment permittivity. The experimental setup of the CSPF-based MMI RI sensor is shown in Fig. 4(a) [28], and the sensitivity of this sensor is enhanced by the efficient excitation of high-order modes and shows ultra-high RI sensitivity. The MMI-based RI fiber sensor is attractive due to the easy fabrication, ultra-high sensitivity, and freedom in tailoring the spectrum.

#### 4.2.2 Humidity sensors

Humidity sensors play an important role in the semiconductor manufacturing process, food storage, structural health monitoring, and meteorology field [113]. The sensitivity and dynamic range are two vital parameters of humidity sensors. Currently, there are multiple sensing techniques to monitor relative humidity (RH) like resistive, capacitive, gravimetric, and optic technologies [114]. Although humidity sensors based on resistive and capacitive

techniques have the advantages of low cost, mass producibility, and broad dynamic range, the sensors based on the gravimetric technique have the advantages of low hysteresis and drift [114, 115]. However, the optical fiber humidity sensor has the characteristics of the compact size, immunity to electromagnetic interference, and suitability for remote sensing and in line monitoring, and it has an irreplaceable role in hazardous environments. The experimental setup for humidity sensing is described in Fig. 4(b). Researchers have been committed to developing high performance humidity sensors, in which SPF humidity sensors based on 2D materials researched by Jinan University show high sensitivity, broad dynamic range, and fast response [114–119]. 2D materials such as transition metal dichalcogenides (TMDs) and graphene oxide (GO), have been applied to the field of sensing because of the high surface to volume ratio and unique optics properties [114, 116]. We enumerate the performance of these SPF humidity sensors in Table 2. The $MoSe_2$ sensor shows a response and recovery time of 1 s and 4 s, which has the capability of monitoring human breath [114].

Table 2 Performance of three types of sensors based on the SPF platform.

| Main measurands | Structures | Mechanism | Sensing range | Sensitivity | Reference |
|---|---|---|---|---|---|
| Refractive index | CSPF | MMI | 1.442 RIU–1.444 RIU | 28000 nm/RIU | [28] |
| | Gold grating coated on side-polished PCF | SPR | 1.36 RIU–1.38 RIU | 3340 nm/RIU | [109] |
| | Gold nano-columns array coated on SPF | SPR | 1.33 RIU–1.39 RIU | 5318 nm/RIU | [112] |
| Relative humidity | Molybdenum diselenide ($MoSe_2$) coated on SPF | | 32% RH–73% RH | 0.321 dB/RH% | [114] |
| | GO film coated on SPF | | 32% RH–85% RH | 0.145 nm/RH% | [116] |
| | Polymer nanostructure coated on SPF | | 30% RH–50% RH | 1.12 nm/RH% | [117] |
| Temperature | PDMS coated on SPF | | 30 ℃–85 ℃ | –0.4412 nm/℃ | [30] |
| | Liquid-filled SPF cavity | MZI | 30 ℃–80 ℃ | –84.72 nm/℃ | [120] |
| | rGO film coated on SPF | | –7.8 ℃–77 ℃ | 0.134 dB/℃ | [122] |

#### 4.2.3 Temperature sensors

Compared with the traditional electric sensors, fiber temperature sensors have the ability of withstanding harsh environments like high temperature and high pressure and the capability of distributed remote measurement [120]. Temperature sensing is usually based on the wavelength shift of the transmission spectrum or the variation of transmitted power. One efficient way to realize high sensitivity is by combining of a sensitive material with the optical waveguide [30, 121, 122]. Reduced graphene oxide (rGO), polystyrene microspheres, and polydimethylsiloxane (PDMS) have ultrahigh thermal conductivity and optical absorption ability, which are very sensitive to temperature variation [30, 122, 123], and the experimental setup of the polystyrene microspheres temperature sensor is shown in Fig. 4(c). The other way to achieve the temperature sensor is by using the Mach-Zehnder interferometer (MZI) structure. We enumerate the performance of the SPF based temperature sensors in Table 2, among them, the MZI-based fiber sensor has ultra-high sensitivity to environmental variations, which is always used for temperature, strain, torsion, and refractive index sensing.

#### 4.2.4 UV/violet sensors

Ultra-violet (UV)/violet sensors are used to in-line and in-situ monitor the optical power levels of violet light or UV light. P-LCs are sensitive to magnetic, electric, thermal, and optic, especially the UV light [95, 96, 124, 125]. In P-LCs based sensors, the deformation of P-LCs molecules can be

transduced and amplified easily [125]. The principle of the UV/violet sensor is that when the light (<450 nm) is incident, the photochemical phase transition of P-LCs generated by the trans-to-cis photoisomerization of azobenzene makes the refractive index of the LCs change. Thanks to the emergence of the SPF, it can be used as a sensing platform to expand the functionalities of P-LCs-based sensing materials. Recently, SPF overlaid hybrid P-LCs (an azobenzene dye, a chiral dopant, and a nematic P-LCs) have been used to UV light sensing which are sensitive to the 380 nm light emitting diode (LED), mercury lamp, and office ceiling lights. The experimental setup is shown in Fig. 4(d) [125]. The sensitivity of this sensor is 0.16 dB/(μW/cm$^2$) with a detection limit of 45 lx when a 380 nm LED light is illuminated. Another fiber optic violet sensor is based on the optical surface grating, which is formed by a P-LC hybrid film covered on the SPF [124]. It shows a loss peak in the transmission spectrum between 1520 nm and 1620 nm, and this loss peak shifts linearly toward the shorter wavelength as the 405 nm light power increases from 30 mW/cm$^2$ to 80 mW/cm$^2$ with a high sensitivity of 1.154 nm (mW·cm$^{-2}$)$^{-1}$.

#### 4.2.5 Strain sensors

Strain sensors are widely used in aerospace, civil engineering, and electric power projects. In recent years, wearable and flexible electronic devices have attracted a great attention. However, due to the poor stretchability and fragility of crystalline silicon, the dominance of semiconductor strain sensors in modern strain sensing has been weakened. In order to meet the surge in demand for flexible electronic sensors, some novel strain sensing techniques have been discovered, such as the carbon nanomaterials based films [126], polymer optical fiber [127], fiber loop mirror [128], Raman spectroscopy [129], and FBG [130]. The SPF has been used in strain sensors due to the strong strength, sustainability, and durability. A D-shaped polarization maintaining fiber loop mirror-based sensor has been presented, which can monitor strain and the surrounding temperature simultaneously [128]. This sensor shows high sensitivities of 46 pm/με and 130 pm/℃ for strain and temperature, respectively. The complete experimental scheme for the proposed sensor is shown in Fig. 4(e). The change of the surrounding medium directly affects the propagation constants or the length of the D-shaped polarization maintaining fiber loop mirror, which is reflected in the power loss or the shift of the peak/dip spectral location [128]. Lo *et al*. [131] proposed an ultrahigh sensitivity ($2.19\times10^4$ deg/ε) polarimetric strain sensor on the D-shaped optical fiber based on the SPR technology. It exhibited significantly higher sensitivity than a non-SPR fiber sensor ($5.2\times10^2$ deg/ε) [131]. Ying *et al*. [132] further discussed the SPR strain sensing characteristics through numerical simulation. Studies have shown that D-shaped optical fiber sensors have better performance and show a great potential for high-sensitivity stain sensors.

#### 4.2.6 Acoustic sensors

The need of acoustic wave detection and analysis have grown a lot in the past few decades, such as in the applications of navigation (depth sounding/sea-bottom profiling), non-destructive evaluation of structures through detection of emitted ultrasounds (detection and location of cracks and inner stresses), and health sciences (medical imaging and diagnosis) [133]. Whether in the air or water, the acoustic pressure is the most common measurement with amplitudes on the order of mPa ($10^{-8}$ bar) [134]. Acoustic methods have the ability to study the structure and properties of materials and their internal physical processes. Fiber-optic acoustic pressure sensors have attracted more interest than common piezoelectric or capacitive sensors due to their advantages of small size, immunity to electromagnetic interference, fast response, and resistance to harsh environments [135]. There are

three dominant technologies in fiber-optic acoustic sensors: FBG, MZI, and Fabry-Perot interferometer configurations [133–136]. Among them, the side-polished FBG acoustic sensor shows an enhanced pressure sensitivity, the acoustic pressure-induced wavelength shift reaches 0.041 nm/Pa, and the noise equivalent acoustic signal level reaches 1.66 mPa/Hz$^{1/2}$ at 2.5 kHz. The schematic diagram of this sensor is shown in Fig. 4(f) [135]. With the development of strain-sensitive nanomaterials, the side-polished FBG shows a potential for developing highly sensitive acousto-ultrasonic sensors in the field of health monitoring and wearables.

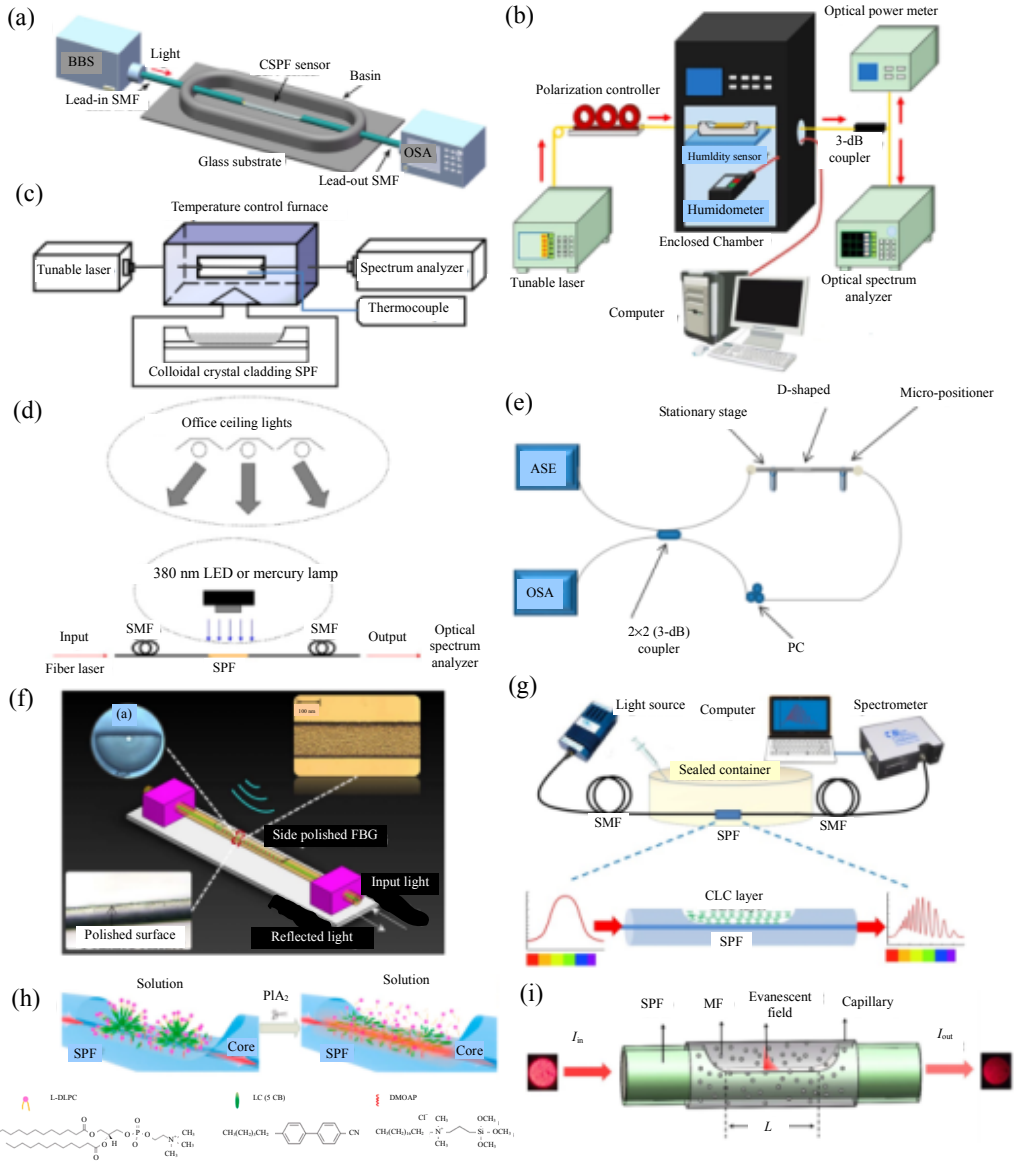


Fig. 4 SPF-based optical sensors: (a) schematic diagram of the experimental setup for the CSPF RI sensor [28], (b) schematic diagram of the experimental setup for humidity sensing [116], (c) schematic diagram of the experimental setup for temperature sensing [123], (d) experimental setup of in-situ detecting the variation of light power by a fiber-optic violet sensor [125], (e) experimental setup of the strain and temperature sensor [128], (f) schematic diagram of the side-polished FBG acoustic sensor and its micrograph [135], (g) schematic diagram of the VOC sensor based on the P-LCs film [137], (h) principle of the fiber sensor for $PLA_2$ detection [144], and (i) schematic diagram of the vector magnetic field sensing unit [147]. VOC: volatile organic compound.

#### 4.2.7 Biological and chemical sensors

Biological and chemical sensing is closely related to human health and safety. The VOCs gas is a common air pollutant that evaporates easily at room temperature [137, 138]. Sensing and monitoring the VOC gas show an important status in human health, industry, and agriculture because of the high flammability and explosion of VOCs. Many sensors have been fabricated to detect VOCs, such as cholesteric P-LCs film sensors [137], rGO sensors [139], metal oxide sensors [140], polymer composite sensors [138, 141], and CNTs (carbon nanotubes) sensors [142]. Among them, SPFs provide a platform to integrate these materials for in line monitoring VOCs in real time. Tang *et al*. [137] designed a wavelength selectively coupling from the SPF to the cholesteric P-LCs film sensor, which was sensitive to tetrahydrofuran, acetone, and methanol gas with the sensitivities of 7.08 nm·L/mmol, 3.46 nm·L/mmol, and 0.52 nm·L/mmol, respectively, as shown in Fig. 4(g). Khan *et al*. [138] deposited a polymer planar waveguide on the SPF to fabricate a high sensitivity and a wide dynamic range sensor with the response time of 35 s, and it could detect dimethylamine, ethanol, benzene, toluene, and acetic acid with the concentration of 0 ppm – 5 ppm. In these wavelength shift VOC sensing systems, the resonance wavelength shifted with the change of the VOC concentration.

SPF-based SPR sensors play a beneficial role in the application of in-situ, real-time, and label-free biosensing applications. Some SPF-based SPR sensors have been realized to detect the bovine serum albumin and phospholipase $A_2$($PLA_2$) in the nM concentration, as shown in Fig. 4(h) [143, 144]. A D-shaped PCF biosensor proposed by Wu *et al*. has shown the sensitivity of 21700 nm/RIU in the refractive index environment of 1.33 – 1.34, and the excellent sensing performance of a D-shaped PCF SPR sensor was experimental demonstrated [50]. Dong *et al*. [21] demonstrated a side polished few-mode fiber SPR biosensor based on the gold film [Fig. 4(f)], the sensitivity reached 4903 nm/RIU, and the figure of merit was 46.1 $RIU^{-1}$ when the RI ranged from 1.333 to 1.404. These provide a potential way for quantitatively detecting biological molecules in a real-time and online manner.

#### 4.2.8 Vector magnetic field sensors

Magnetic field sensors are important to the areas of industry and military. However, the applications are limited because they can only sense the intensity of the magnetic field and cannot determine the direction [145]. The non-central symmetric structure of the SPF provides a new approach to detect the intensity and the orientation of the magnetic field simultaneously [9, 146, 147]. Combining SPFs with the SPR technology helps to construct highly-sensitive magnetic-field sensors, and several works have already been published [9, 146]. Jiang *et al*. [9] proposed an SPF-based SPR vector magnetic field sensor, and the sensor showed a high sensitivity of 598.7 pm/Oe to the magnetic field intensity and a sensitivity of –5.63 nm/deg to the orientation of the magnetic field. Chen *et al*. [146] developed a highly-sensitive vector magnetometer based on the side-polished few-mode-fiber and SPR technology, and it is sensitive to the intensity and orientation of magnetic field (0.692 nm/Oe and –11.917 nm/deg, respectively). Chen *et al*. [147] further proposed a portable vector-magnetometer based on the SPF and smartphone platform, and the sensitivities of this magnetometer to the intensity and orientation of the magnetic field can reach –0.050 dB/Oe and –0.263 dB/deg, respectively, as shown in Fig. 4(i). This portable, low-cost, and highly-sensitive vector-magnetometer is suitable for sensing magnetic vector applications that require a portable size and real-time transmission of the measured results.

## 5. Conclusions and prospective future

This article reviews and summarizes the

fabricating technique, fiber types, characteristics, and applications of SPFs, which have aroused strong interests and exhibited excellent application potentials in optical fiber devices and sensors. The SPF, an excellent versatile platform, has realized the integration with multiple materials such as metals, 2D materials, and P-LCs. The SPF can enhance the light-matter interaction, making the "lab-on-fiber" possible. Now, the fully automatic artificial intelligence fabrication technology and equipment have been successfully developed and commercialized, ensuring the large-scale fabrication and commercial application of the SPF. The applications of the SPF based devices and sensors have been intensively studied in the following areas: optical communication, WDM, health monitoring and wearables, environmental real-time monitoring, and detection of chemical substances and specific biological targets in the food and medical field.

## Acknowledgment

The authors would like to thank the editor and the reviewers for their valuable comments and suggestions, which help improve the quality of the paper. This work is supported by the National Natural Science Foundation of China (Grant Nos. 12174155, 61705086, 61675092, and 62075088), National Key Research and Development Program of China (Grant Nos. 2021YFB2800801 and 2018YFB1801900), Natural Science Foundation of Guangdong Province for Distinguished Young Scholar (Grant No. 2020B1515020024), Natural Science Foundation of Guangdong Province (Grant Nos. 2017A030313375 and 2019A1515011380), Key-Area Research and Development Program of Guangdong Province (Grant No. 2019B010138004), Project of Guangzhou Industry Leading Talents (Grant No. CXLJTD-201607), Aeronautical Science Foundation of China (Grant Nos. 201708W4001 and 201808W4001), and Project of STRPAT of EC Laboratory (Grant No. ZHD201902), TESTBED2 (Grant No. H2020-MSCA-RISE-2019), and Jinan Outstanding Young Scholar Support Program (Grant Nos. JNSBYC-2020040 and JNSBYC-2020117).



## References

[1] J. S. Levy, A. Gondarenko, M. A. Foster, A. C. Turner-Foster, A. L. Gaeta, and M. Lipson, "CMOS-compatible multiple-wavelength oscillator for on-chip optical interconnects," *Nature Photonics*, 2010, 4(1): 37–40.

[2] P. Sibson, J. E. Kennard, S. Stanisic, C. Erven, J. L. O'Brien, and M. G. Thompson, "Integrated silicon photonics for high-speed quantum key distribution," *Optica*, 2017, 4(2): 172–177.

[3] M. J. Paniccia, "A perfect marriage: optics and silicon: integrated silicon-based photonics now running at 50 Ggps, with terabit speeds on the horizon," *Optik & Photonik*, 2011, 6(2): 34–38.

[4] M. Consales, A. Ricciardi, A. Crescitelli, E. Esposito, A. Cutolo, and A. Cusano, "Lab-on-fiber technology: toward multifunctional optical nanoprobes," *ACS Nano*, 2012, 6(4): 3163–3170.

[5] M. Consales, M. Pisco, and A. Cusano, "Lab-on-fiber technology: a new avenue for optical nanosensors," *Photonic Sensors*, 2012, 2(4): 289–314.

[6] A. Ricciardi, A. Crescitelli, P. Vaiano, G. Quero, M. Consales, M. Pisco, *et al.*, "Lab-on-fiber technology: a new vision for chemical and biological sensing," *Analyst*, 2015, 140(24): 8068–8079.

[7] A. O. Dikovska, G. Atanasova, N. Nedyalkov, P. Stefanov, P. Atanasov, E. Karakoleva, *et al.*, "Optical sensing of ammonia using ZnO nanostructure grown on a side-polished optical-fiber," *Sensors and Actuators B: Chemical*, 2010, 146(1): 331–336.

[8] J. Zhao, S. Cao, C. Liao, Y. Wang, G. Wang, X. Xu, *et al.*, "Surface plasmon resonance refractive sensor based on silver-coated side-polished fiber," *Sensors and Actuators B: Chemical*, 2016, 230: 206–211.

[9] Z. Jiang, J. Dong, S. Hu, Y. Zhang, Y. Chen, Y. Luo, *et al.*, "High-sensitivity vector magnetic field sensor based on side-polished fiber plasmon and ferrofluid," *Optics Letters*, 2018, 43(19): 4743–4746.

[10] L. Dong, X. Liu, Y. Zhang, L. Zhuo, D. Li, W. Zhu,

*et al.*, "All-fiber multifunctional electrooptic prototype device with a graphene/PMMA (poly (methyl methacrylate)) hybrid film integrated on coreless side-polished fibers," *ACS Applied Electronic Materials*, 2020, 2(2): 447–455.

[11] L. Zhuo, P. Fan, S. Zhang, X. Liu, X. Guo, Y. Zhang, *et al.*, "A broadband all-fiber integrated graphene photodetector with CNT-enhanced responsivity," *Nanoscale*, 2020, 12(26): 14188–14193.

[12] S. Masuda and T. Iwama, "Single-mode fiber-optic directional coupler," *Applied Optics*, 1982, 21(19): 3484–3488.

[13] S. M. Tseng and C. L. Chen, "Side-polished fibers," *Applied Optics*, 1992, 31(18): 3438–3447.

[14] L. Pei, R. Zhao, T. Ning, C. Qi, and J. Li, "Key technologies for side-grinding optical fiber with long length and high precision and their applications," *Infrared and Laser Engineering*, 2010, 1: 86–90.

[15] A. O. Dikovska, P. Atanasov, A. T. Andreev, B. Zafirova, E. Karakoleva, and T. Stoyanchov, "ZnO thin film on side polished optical fiber for gas sensing applications," *Applied Surface Science*, 2007, 254(4): 1087–1090.

[16] S. S. Lee, H. D. Chae, D. H. Kim, H. J. Kim, and K. T. Kim, "Continuous photonic microwave true-time delay using a side-polished fiber Bragg grating with heating electrode," *Microwave and Optical Technology Letters*, 2005, 44(1): 35–37.

[17] C. Hussey and J. Minelly, "Optical fibre polishing with a motor-driven polishing wheel," *Electronics Letters*, 1988, 24(13): 805–807.

[18] N. A. M. Zainuddin, M. M. Ariannejad, P. T. Arasu, S. W. Harun, and R. Zakaria, "Investigation of cladding thicknesses on silver SPR based side-polished optical fiber refractive-index sensor," *Results in Physics*, 2019, 13: 102255.

[19] J. Tang, J. Zhou, J. Guan, S. Long, J. Yu, H. Guan, *et al.*, "Fabrication of side-polished single mode-multimode-single mode fiber and its characteristics of refractive index sensing," *IEEE Journal of Selected Topics in Quantum Electronics*, 2016, 23(2): 238–245.

[20] R. King, F. Seng, N. Stan, K. Cuzner, C. Josephson, R. Selfridge, *et al.*, "Slab-coupled optical sensor fabrication using side-polished Panda fibers," *Applied Optics*, 2016, 55(31): 8848–8854.

[21] J. Dong, Y. Zhang, Y. Wang, F. Yang, S. Hu, Y. Chen, *et al.*, "Side-polished few-mode fiber based surface plasmon resonance biosensor," *Optics Express*, 2019, 27(8): 11348–11360.

[22] L. Bilro, N. J. Alberto, L. M. Sá, J. de Lemos Pinto, and R. Nogueira, "Analytical analysis of side-polished plastic optical fiber as curvature and refractive index sensor," *Journal of Lightwave Technology*, 2011, 29(6): 864–870.

[23] M. Cordaro, D. L. Rode, T. Barry, and R. R. Krchnavek, "Precision fabrication of D-shaped single-mode optical fibers by in situ monitoring," *Journal of Lightwave Technology*, 1994, 12(9): 1524–1531.

[24] H. Ahmad, H. Hassan, A. Zulkifli, K. Thambiratnam, and I. Amiri, "Characterization of arc-shaped side-polished fiber," *Optical and Quantum Electronics*, 2017, 49(6): 207.

[25] J. Zhao, G. Yin, C. Liao, S. Liu, J. He, B. Sun, *et al.*, "Rough side-polished fiber with surface scratches for sensing applications," *IEEE Photonics Journal*, 2015, 7(3): 1–7.

[26] Y. Xiao, Z. Chen, L. Zhang, J. Zhang, J. Qin, and H. Pan, "All fiber online optical power monitor based on side-polished fiber," *Journal of Applied Optics*, 2010, 31(4): 620–625.

[27] Z. Chen and C. Bai, "Effect of overlaid material on optical transmission of side-polished fiber made by wheel side polishing," in *2008 1st Asia-Pacific Optical Fiber Sensors Conference*, China, 2008, pp. 1–4.

[28] H. Dong, L. Chen, J. Zhou, J. Yu, H. Guan, W. Qiu, *et al.*, "Coreless side-polished fiber: a novel fiber structure for multimode interference and highly sensitive refractive index sensors," *Optics Express*, 2017, 25(5): 5352–5365.

[29] M. J. Digonnet, J. Feth, L. F. Stokes, and H. J. Shaw, "Measurement of the core proximity in polished fiber substrates and couplers," *Optics Letters*, 1985, 10(9): 463–465.

[30] C. He, J. Fang, Y. Zhang, Y. Yang, J. Yu, J. Zhang, *et al.*, "High performance all-fiber temperature sensor based on coreless side-polished fiber wrapped with polydimethylsiloxane," *Optics Express*, 2018, 26(8): 9686–9699.

[31] C. Bai, Y. Luo, Z. Chen, X. Chen, M. Xu, and J. Tang, "Characteristics of side-polished fiber in refractive index sensing," *Acta Photonica Sinica*, 2013, 42(10): 1182.

[32] C. Bai, Z. Chen, F. Li, Y. Zhang, Y. Zeng, and L. Liu, "Experimental investigations of transmitting optical power in side-polished fiber," *Acta Photonica Sinica*, 2007, 36(6): 1068.

[33] Y. Xiao, J. Zhang, J. Yu, H. Dong, Y. Wei, Y. Luo, *et al.*, "Theoretical investigation of optical modulators based on graphene-coated side-polished fiber," *Optics Express*, 2018, 26(11): 13759–13772.

[34] J. Tang, J. Zhou, J. Guan, S. Long, J. Yu, H. Guan, *et al.*, "Fabrication of side-polished single mode-multimode-single mode fiber and its characteristics of refractive index sensing," *IEEE Journal of Selected Topics in Quantum Electronics*, 2016, 23(2): 238–245.

[35] G. Mu, Y. Liu, Q. Qin, Z. Tan, G. Li, M. Wang, *et al.*, "Refractive index sensing based on the analysis of D-shaped multimode fiber specklegrams," *IEEE Photonics Technology Letters*, 2020, 32(8): 485–488.

[36] M. Yang, H. Liu, D. Zhang, and X. Tong, "Hydrogen

sensing performance comparison of Pd layer and Pd/$WO_3$ composite thin film coated on side-polished single-and multimode fibers," *Sensors and Actuators B: Chemical*, 2010, 149(1): 161–164.
[37] R. Ranjan, F. Esposito, S. Campopiano, and A. Iadicicco, "Sensing characteristics of arc-induced long period gratings in polarization-maintaining panda fiber," *IEEE Sensors Journal*, 2017, 17(21): 6953–6959.
[38] W. Zheng, "Automated fusion-splicing of polarization maintaining fibers," *Journal of Lightwave Technology*, 1997, 15(1): 125–134.
[39] D. Wang, C. Liu, X. Shu, X. Mou, and G. Yang, "Accurate alignment of PM fiber," *Acta Photonica Sinica*, 2002, 31(3): 345.
[40] Z. Liu, D. Feng, H. Huang, D. Yang, and N. Song, "Automatic aligning method of panda polarization maintaining fiber with high accuracy," *Acta Photonica Sinica*, 2015, 44(2): 206004.
[41] K. Itoh, N. Yoshinuma, N. Suzuji, T. Yamada, and H. Taya, "Method of fusion-splicing polarization maintaining optical fibers," U.S. Patent 5 013 345, May 7, 1991.
[42] J. Wang, Z. Lin, Y. Wu, and S. Li, "The auto-alignment technique of PM fiber of MRI," *Journal of Applied Optics*, 2005, 26(5): 37–40.
[43] S. Chen, "Azimuthal alignment method for PM fiber based on light intensity distributions with five finger profile," *Applied Laser*, 2006, 26(1): 35–38.
[44] L. Huang, J. Zhang, Z. Chen, and S. Chen, "Simulation and experiments analysis of azimuth aligning technology for polarization maintaining fiber," *Infrared and Laser Engineering*, 2010, 2: 279–284.
[45] K. T. Kim, D. S. Yoon, and G. Kwoen, "Optical properties of side-polished polarization maintaining fiber coupled with a high index planar waveguide," *Optics Communications*, 2004, 230(1–3): 137–144.
[46] G. Du, "Experimental research on F-P cavity Raman fiber laser," *Acta Photonica Sinica*, 2004, 33(9): 1151.
[47] M. Piliarik, J. Homola, Z. Manıková, and J. Čtyroký, "Surface plasmon resonance sensor based on a single-mode polarization-maintaining optical fiber" *Sensors and Actuators B: Chemical*, 2003, 90(1–3): 236–242.
[48] T. Wu, Z. Liu, H. Zhang, Z. Yang, D. Yang, and Y. Wang, "Investigation of side-polished panda fibers for strain measurement and surface plasmon resonance-based biochemical sensing," in *2020 IEEE International Conference on Parallel & Distributed Processing with Applications, Big Data & Cloud Computing, Sustainable Computing & Communications, Social Computing & Networking (ISPA/BDCloud/SocialCom/SustainCom)*, China, 2020, pp. 1334–1341.
[49] W. Zhu, S. Long, Z. Gan, Y. Luo, Y. Ma, H. Guan, *et al.*, "Optimization of polishing parameters for optical coupler based on side-polished photonic crystal fiber," *Optical and Quantum Electronics*, 2017, 49(2): 81.
[50] T. Wu, Y. Shao, Y. Wang, S. Cao, W. Cao, F. Zhang, *et al.*, "Surface plasmon resonance biosensor based on gold-coated side-polished hexagonal structure photonic crystal fiber," *Optics Express*, 2017, 25(17): 20313–20322.
[51] N. Zhang, G. Humbert, Z. Wu, K. Li, P. P. Shum, N. M. Y. Zhang, *et al.*, "In-line optofluidic refractive index sensing in a side-channel photonic crystal fiber," *Optics Express*, 2016, 24(24): 27674–27682.
[52] J. N. Dash and R. Jha, "Highly sensitive side-polished birefringent PCF-based SPR sensor in near IR," *Plasmonics*, 2016, 11(6): 1505–1509.
[53] D. Li, S. Pu, Y. Zhao, Y. Li, Z. Hao, and Z. Han, "Sensing properties of symmetrical side-polished photonic crystal fiber based on surface plasmon resonance," *Optik*, 2020, 224: 165662.
[54] X. He, Z. Chen, J. Yu, Y. Zeng, Y. Luo, J. Zhang, *et al.*, "Numerical analysis of optical propagation characteristics of side-polished photonics crystal fiber," *Optical and Quantum Electronics*, 2014, 46(10): 1261–1268.
[55] Z. Naqvi, M. Green, C. Wang, and T. H. Her, "Characterization of Bragg fibers by Mie scattering," *CLEO: Applications and Technology*, 2016, DOI: 10.1364/CLEO_AT.2016.JTu5A.112.
[56] P. Yan, J. Zhao, S. Ruan, J. Zhao, G. Du, H. Wei, *et al.*, "Improved large-mode-area Bragg fiber," *Chinese Optics Letters*, 2011, 9(6): 060603.
[57] L. Shi, W. Zhang, J. Jin, Y. Huang, and J. Peng, "Hollow-core Bragg fiber and its application in trace gas sensing," in *Asia Communications and Photonics Conference and Exhibition*, America, 2010, pp. 799008.
[58] J. Jiang, G. M. Ma, C. R. Li, H. T. Song, Y. T. Luo, and H. B. Wang, "Highly sensitive dissolved hydrogen sensor based on side-polished fiber Bragg grating," *IEEE Photonics Technology Letters*, 2015, 27(13): 1453–1456.
[59] M. Yang, J. Dai, X. Li, and J. Wang, "Side-polished fiber Bragg grating refractive index sensor with TbFeCo magnetoptic thin film," *Journal of Applied Physics*, 2010, 108(3): 033102.
[60] Y. Ying, R. Zhang, G. Y. Si, X. Wang, and Y. W. Qi, "D-shaped tilted fiber Bragg grating using magnetic fluid for magnetic field sensor," *Optics Communications*, 2017, 405: 228–232.
[61] N. Jing, J. Zheng, X. Zhao, and C. Teng, "Refractive index sensing based on a side-polished macrobending plastic optical fiber," *IEEE Sensors Journal*, 2014, 15(5): 2898–2901.
[62] L. Bilro, N. Alberto, J. L. Pinto, and R. Nogueira, "Optical sensors based on plastic fibers," *Sensors*, 2012, 12(9): 12184–12207.

[63] P. Stajanca, O. Cetinkaya, M. Schukar, P. Mergo, D. J. Webb, and K. Krebber, "Molecular alignment relaxation in polymer optical fibers for sensing applications," *Optical Fiber Technology*, 2016, 28: 11–17.

[64] Y. Wakayama, J. Ko, N. Yoshikane, and T. Tsuritani, "Pure-silica single-core to multi-core fiber coupler with side-polishing approach," in *2020 Opto-Electronics and Communications Conference (OECC)*, China, 2020, pp. 1–3.

[65] Y. Bo, C. Guan, R. Chu, T. Cheng, L. Xu, and L. Liu, "Compact all-fiber thermo-optic modulator based on a Michelson interferometer coated with $NaNdF_4$ nanoparticles," *Optics Express*, 2021, 29(5): 6854–6862.

[66] R. Chu, C. Guan, Y. Bo, J. Liu, J. Shi, J. Yang, *et al.*, "Graphene decorated twin-core fiber Michelson interferometer for all-optical phase shifter and switch," *Optics Letters*, 2020, 45(1): 177–180.

[67] J. Yang, C. Guan, Z. Yu, M. Yang, J. Shi, P. Wang, *et al.*, "High sensitivity humidity sensor based on gelatin coated side-polished in-fiber directional coupler," *Sensors and Actuators B: Chemical*, 2020, 305: 127555.

[68] I. Yokohama, J. Noda, and K. Okamoto, "Fiber-coupler fabrication with automatic fusion-elongation processes for low excess loss and high coupling-ratio accuracy," *Journal of Lightwave Technology*, 1987, 5(7): 910–915.

[69] M. V. Hernandez-Arriaga, M. A. Bello-Jimenez, A. Rodríguez-Cobos, R. López-Estopier, and M. V. Andres, "High sensitivity refractive index sensor based on highly overcoupled tapered fiber-optic couplers," *IEEE Sensors Journal*, 2016, 17(2): 333–339.

[70] K. Zhang, P. Wu, J. Dong, D. Du, Z. Yang, C. Xu, *et al.*, "Broadband mode-selective couplers based on tapered side-polished fibers," *Optics Express*, 2021, 29(13): 19690–19702.

[71] H. Kim, J. Kim, U. C. Paek, B. H. Lee, and K. T. Kim, "Tunable photonic crystal fiber coupler based on a side-polishing technique," *Optics Letters*, 2004, 29(11): 1194–1196.

[72] Y. Luo, Q. Wei, Y. Ma, H. Lu, J. Yu, J. Tang, *et al.*, "Side-polished-fiber based optical coupler assisted with a fused nano silica film," *Applied Optics*, 2015, 54(7): 1598–1605.

[73] V. R. K. Kumar, A. George, W. Reeves, J. Knight, P. S. J. Russell, F. Omenetto, *et al.*, "Extruded soft glass photonic crystal fiber for ultrabroad supercontinuum generation," *Optics Express*, 2002, 10(25): 1520–1525.

[74] B. H. Almewafy, N. F. Areed, M. F. O. Hameed, and S. S. Obayya, "Modified D-shaped SPR PCF polarization filter at telecommunication wavelengths," *Optical and Quantum Electronics*, 2019, 51(6): 1–14.

[75] R. Wu, H. Chen, S. Zhang, H. Fu, Z. Luo, L. Zhang, *et al.*, "Tunable and selectable multipassband microwave photonic filter utilizing reflective and cascaded fiber Mach-Zehnder interferometers," *Journal of Lightwave Technology*, 2017, 35(13): 2660–2668.

[76] J. Yu, Y. Han, H. Huang, H. Li, V.K. Hsiao, W. Liu, *et al.*, "All-optically reconfigurable and tunable fiber surface grating for in-fiber devices: a wideband tunable filter," *Optics Express*, 2014, 22(5): 5950–5961.

[77] J. L. Archambault, P. S. J. Russell, S. Barcelos, P. Hua, and L. Reekie, "Novel channel-dropping filter by grating-frustrated coupling in single-mode optical fiber," in *Optical Fiber Communication Conference*, America, 1994, pp. TuL5.

[78] R. Lausten, P. Rochon, M. Ivanov, P. Cheben, S. Janz, P. Desjardins, *et al.*, "Optically reconfigurable azobenzene polymer-based fiber Bragg filter," *Applied Optics*, 2005, 44(33): 7039–7042.

[79] J. Yu, S. Jin, Q. Wei, Z. Zang, H. Lu, X. He, *et al.*, "Hybrid optical fiber add-drop filter based on wavelength dependent light coupling between micro/nano fiber ring and side-polished fiber," *Scientific Reports*, 2015, 5(1): 1–6.

[80] T. Sherwood, A. C. Young, J. Takayesu, A. K. Jen, L. R. Dalton, and A. Chen, "Microring resonators on side-polished optical fiber," *IEEE Photonics Technology Letters*, 2005, 17(10): 2107–2109.

[81] L. Shi, Q. Wang, and T. Zhu, "A fiber-attached coupler for transmission bandpass whispering gallery mode resonator," *Journal of Lightwave Technology*, 2021, 39(8): 2454–2459.

[82] L. Shi, T. Zhu, D. Huang, M. Liu, M. Deng, and W. Huang, "In-fiber whispering-gallery-mode resonator fabricated by femtosecond laser micromachining," *Optics Letters*, 2015, 40(16): 3770–3773.

[83] T. Sherwood, A. C. Young, J. Takayesu, A. K. Y. Jen, L. R. Dalton, and A. Chen, "Microring resonators on side-polished optical fiber," *IEEE Photonics Technology Letters*, 2005, 17(10): 2107–2109.

[84] L. Shi, Q. Wang, L. Jiang, Q. Gao, and T. Zhu, "In-fiber butt-coupled spherical microcavity with whispering gallery mode and Fabry-Perot resonances," *IEEE Photonics Technology Letters*, 2021, 33(11): 553–556.

[85] S. Lee, J. Sokoloff, B. McGinnis, and H. Sasabe, "Fabrication of a side-polished fiber polarizer with a birefringent polymer overlay," *Optics Letters*, 1997, 22(9): 606–608.

[86] X. Wang, J. Lin, W. Sun, Z. Tan, R. Liu, and Z. Wang, "Polarization selectivity of the thin-metal-film plasmon-assisted fiber-optic polarizer," *ACS Applied Materials & Interfaces*, 2020, 12(28): 32189–32196.

[87] R. A. Bergh, H. C. Lefevre, and H. J. Shaw,

"Single-mode fiber-optic polarizer," *Optics Letters*, 1980, 5(11): 479–481.

[88] M. Heidari, V. Faramarzi, Z. Sharifi, M. Hashemi, S. Bahadori-Haghighi, B. Janjan, *et al.*, "A high-performance TE modulator/TM-pass polarizer using selective mode shaping in a $VO_2$-based side-polished fiber," *Nanophotonics*, 2021, 10(13): 3451–3463.

[89] Q. Bao, H. Zhang, B. Wang, Z. Ni, C. Lim, Y. Wang, *et al.*, "Broadband graphene polarizer," *Nature Photonics*, 2011, 5(7): 411–415.

[90] R. Chu, C. Guan, J. Yang, Z. Zhu, P. Li, J. Shi, *et al.*, "High extinction ratio D-shaped fiber polarizers coated by a double graphene/PMMA stack," *Optics Express*, 2017, 25(12): 13278–13285.

[91] W. Li, L. Yi, R. Zheng, Z. Ni, and W. Hu, "Fabrication and application of a graphene polarizer with strong saturable absorption," *Photonics Research*, 2016, 4(2): 41–44.

[92] L. Zhuo, D. Li, W. Chen, Y. Zhang, W. Zhang, Z. Lin, *et al.*, "High performance multifunction-in-one optoelectronic device by integrating graphene/$MoS_2$ heterostructures on side-polished fiber," *Nanophotonics*, 2022, DOI: 10.1515/nanoph-2021-0688.

[93] J. Zhao, Y. Ma, and R. Li, "Characterization of polarizer made of the deep-UV birefringent crystal $Ba_2Mg(B_3O_6)_2$," *Applied Optics*, 2015, 54(33): 9949–9953.

[94] A. Duduś, R. Blue, M. Zagnoni, G. Stewart, and D. Uttamchandani, "Modeling and characterization of an electrowetting-based single-mode fiber variable optical attenuator," *IEEE Journal of Selected Topics in Quantum Electronics*, 2014, 21(4): 253–261.

[95] V. K. Hsiao, Z. Li, Z. Chen, P. C. Peng, and J. Tang, "Optically controllable side-polished fiber attenuator with photoresponsive liquid crystal overlay," *Optics Express*, 2009, 17(22): 19988–19995.

[96] T. Martins, B. Gholipour, D. Piccinotti, K. F. MacDonald, A. C. Peacock, O. Frazão, *et al.*, "Fiber-integrated phase-change reconfigurable optical attenuator," *APL Photonics*, 2019, 4(11): 111301.

[97] H. Knape and W. Margulis, "All-fiber polarization switch," *Optics Letters*, 2007, 32(6): 614–616.

[98] L. Fang and J. Wang, "All-fiber polarization beam splitting and rotating based on vector-mode-assisted coupling," *Optics Express*, 2018, 26(12): 15124–15137.

[99] V. K. Hsiao, W. H. Fu, C. Y. Huang, Z. Chen, S. Li, J. Yu, *et al.*, "Optically switchable all-fiber optic polarization rotator," *Optics Communications*, 2012, 285(6): 1155–1158.

[100] S. C. Wen, C. W. Chang, C. M. Lin, H. Liu, V. K. Hsiao, J. Yu, *et al.*, "Light-induced switching of a chalcogenide-coated side-polished fiber device," *Optics Communications*, 2015, 334: 110–114.

[101] L. Zhuo, P. Fan, S. Zhang, Y. Zhan, Y. Lin, Y. Zhang, *et al.*, "High-performance fiber-integrated multifunctional graphene-optoelectronic device with photoelectric detection and optic-phase modulation," *Photonics Research*, 2020, 8(12): 1949–1957.

[102] Y. Wang, H. Liu, Y. Wang, W. Qiu, J. Zhang, Z. Tian, *et al.*, "Side polished fiber with coated graphene sheet and its control characteristic of violet light," *Optical Materials Express*, 2016, 6(6): 2088–2094.

[103] E. J. Lee, S. Y. Choi, H. Jeong, N. H. Park, W. Yim, M. H. Kim, *et al.*, "Active control of all-fibre graphene devices with electrical gating," *Nature Communications*, 2015, 6(1): 1–6.

[104] Y. Liu, J. Yin, P. Wang, Q. Hu, Y. Wang, Y. Xie, *et al.*, "High-performance, ultra-broadband, ultraviolet to terahertz photodetectors based on suspended carbon nanotube films," *ACS Applied Materials & Interfaces*, 2018, 10(42): 36304–36311.

[105] Y. Zhang, T. Liu, B. Meng, X. Li, G. Liang, X. Hu, *et al.*, "Broadband high photoresponse from pure monolayer graphene photodetector," *Nature Communications*, 2013, 4(1): 1–11.

[106] S. Cakmakyapan, P. K. Lu, A. Navabi, and M. Jarrahi, "Gold-patched graphene nano-stripes for high-responsivity and ultrafast photodetection from the visible to infrared regime," *Light: Science & Applications*, 2018, 7(1): 1–9.

[107] Y. Liu, Q. Xia, J. He, and Z. Liu, "Direct observation of high photoresponsivity in pure graphene photodetectors," *Nanoscale Research Letters*, 2017, 12(1): 1–8.

[108] H. Dong, J. Yu, H. Guan, W. Qiu, J. Dong, H. Lu, *et al.*, "Coreless side-polished fiber for multimode interference and highly sensitive refractive index sensing," *Optics Express*, 2017, 25(5): 5352–5365.

[109] J. Lu, Y. Li, Y. Han, Y. Liu, and J. Gao, "D-shaped photonic crystal fiber plasmonic refractive index sensor based on gold grating," *Applied Optics*, 2018, 57(19): 5268–5272.

[110] J. Wu, S. Li, X. Wang, M. Shi, X. Feng, and Y. Liu, "Ultrahigh sensitivity refractive index sensor of a D-shaped PCF based on surface plasmon resonance," *Applied Optics*, 2018, 57(15): 4002–4007.

[111] P. O. Patil, G. R. Pandey, A. G. Patil, V. B. Borse, P. K. Deshmukh, D. R. Patil, *et al.*, "Graphene-based nanocomposites for sensitivity enhancement of surface plasmon resonance sensor for biological and chemical sensing: a review," *Biosensors and Bioelectronics*, 2019, 139: 111324.

[112] M. Yang, S. Long, W. Zhu, Y. Luo, P. Mao, J. Tang, *et al.*, "Design and optimization of nano-column array based surface plasmon resonance sensor," *Optical and Quantum Electronics*, 2017, 49(1):

1–7.

[113] L. Zhang, F. Gu, J. Lou, X. Yin, and L. Tong, "Fast detection of humidity with a subwavelength-diameter fiber taper coated with gelatin film," *Optics Express*, 2008, 16(17): 13349–13353.

[114] T. Ouyang, L. Lin, K. Xia, M. Jiang, Y. Lang, H. Guan, *et al.*, "Enhanced optical sensitivity of molybdenum diselenide ($MoSe_2$) coated side polished fiber for humidity sensing," *Optics Express*, 2017, 25(9): 9823–9833.

[115] A. Tripathy, S. Pramanik, J. Cho, and J. Santhosh, and N. A. A. Osman, "Role of morphological structure, doping, and coating of different materials in the sensing characteristics of humidity sensors," *Sensors*, 2014, 14(9): 16343–16422.

[116] Y. Huang, W. Zhu, Z. Li, G. Chen, L. Chen, J. Zhou, *et al.*, "High-performance fibre-optic humidity sensor based on a side-polished fibre wavelength selectively coupled with graphene oxide film," *Sensors and Actuators B: Chemical*, 2018, 255: 57–69.

[117] L. Tang, Y. Feng, Z. Xing, Z. Chen, J. Yu, H. Guan, *et al.*, "High-sensitivity humidity sensing of side-polished optical fiber with polymer nanostructure cladding," *Applied Optics*, 2018, 57(10): 2539–2544.

[118] Y. Luo, C. Chen, K. Xia, S. Peng, H. Guan, J. Tang, *et al.*, "Tungsten disulfide ($WS_2$) based all-fiber-optic humidity sensor," *Optics Express*, 2016, 24(8): 8956–8966.

[119] D. Li, H. Lu, W. Qiu, J. Dong, H. Guan, W. Zhu, *et al.*, "Molybdenum disulfide nanosheets deposited on polished optical fiber for humidity sensing and human breath monitoring," *Optics Express*, 2017, 25(23): 28407–28416.

[120] H. Zhang, S. Gao, Y. Luo, Z. Chen, S. Xiong, L. Wan, *et al.*, "Ultrasensitive Mach-Zehnder interferometric temperature sensor based on liquid-filled D-shaped fiber cavity," *Sensors*, 2018, 18(4): 1239.

[121] H. Lu, Z. Tian, H. Yu, B. Yang, G. Jing, G. Liao, *et al.*, "Optical fiber with nanostructured cladding of $TiO_2$ nanoparticles self-assembled onto a side polished fiber and its temperature sensing," *Optics Express*, 2014, 22(26): 32502–32508.

[122] J. Zhang, G. Liao, S. Jin, D. Cao, Q. Wei, H. Lu, *et al.*, "All-fiber-optic temperature sensor based on reduced graphene oxide," *Laser Physics Letters*, 2014, 11(3): 035901.

[123] S. Li, L. Xia, Z. Chen, J. Yu, H. Guan, H. Lu, *et al.*, "Colloidal crystal cladding fiber based on side-polished fiber and its temperature sensing" *Optical and Quantum Electronics*, 2017, 49(2): 1–10.

[124] J. Yu, H. Li, V. Hsiao, W. Liu, J. Tang, Y. Zhai, *et al.*, "A fiber-optic violet sensor by using the surface grating formed by a photosensitive hybrid liquid crystal film on side-polished fiber," *Measurement Science and Technology*, 2013, 24(9): 094019.

[125] W. H. Fu, V. K. Hsiao, J. Y. Tang, M. H. Wu, and Z. Chen, "All fiber-optic sensing of light using side-polished fiber overlaid with photoresponsive liquid crystals," *Sensors and Actuators B: Chemical*, 2011, 156(1): 423–427.

[126] M. J. Yee, N. Mubarak, E. Abdullah, M. Khalid, R. Walvekar, R. R. Karri, *et al.*, "Carbon nanomaterials based films for strain sensing application – a review," *Nano-Structures & Nano-Objects*, 2019, 18: 100312.

[127] S. Liehr, P. Lenke, M. Wendt, K. Krebber, M. Seeger, E. Thiele, *et al.*, "Polymer optical fiber sensors for distributed strain measurement and application in structural health monitoring," *IEEE Sensors Journal*, 2009, 9(11): 1330–1338.

[128] H. H. Qazi, A. B. Mohammad, H. Ahmad, and M. Z. Zulkifli, "D-shaped polarization maintaining fiber sensor for strain and temperature monitoring," *Sensors*, 2016, 16(9): 1505.

[129] A. P. A. Raju, A. Lewis, B. Derby, R. J. Young, I. A. Kinloch, R. Zan, *et al.*, "Wide-area strain sensors based upon graphene-polymer composite coatings probed by Raman spectroscopy," *Advanced Functional Materials*, 2014, 24(19): 2865–2874.

[130] D. Song, Q. Chai, Y. Liu, Y. Jiang, J. Zhang, W. Sun, *et al.*, "A simultaneous strain and temperature sensing module based on FBG-in-SMS," *Measurement Science and Technology*, 2014, 25(5): 055205.

[131] Y. L. Lo, C. H. Chuang, and Z. W. Lin, "Ultrahigh sensitivity polarimetric strain sensor based upon D-shaped optical fiber and surface plasmon resonance technology," *Optics Letters*, 2011, 36(13): 2489–2491.

[132] Y. Ying, J. K. Wang, K. Xu, and G. Y. Si, "High sensitivity D-shaped optical fiber strain sensor based on surface plasmon resonance," *Optics Communications*, 2020, 460: 125147.

[133] J. G. Teixeira, I. T. Leite, S. Silva, and O. Frazão, "Advanced fiber-optic acoustic sensors," *Photonic Sensors*, 2014, 4(3): 198–208.

[134] B. Fischer and E. Wintner, "Ultra-sensitive (acoustic) pressure sensor with high temporal resolution," *Optical Sensors*, 2011, DOI: 10.1364/SENSORS.2011.SMB5.

[135] C. Li, X. Peng, H. Zhang, C. Wang, S. Fan, and S. Cao, "A sensitivity-enhanced flexible acoustic sensor using side-polished fiber Bragg grating," *Measurement*, 2018, 117: 252–257.

[136] W. Wang, N. Wu, Y. Tian, X. Wang, C. Niezrecki, and J. Chen, "Optical pressure/acoustic sensor with precise Fabry-Perot cavity length control using angle polished fiber," *Optics Express*, 2009, 17(19):

16613–16618.

[137] J. Tang, J. Fang, Y. Liang, B. Zhang, Y. Luo, X. Liu, *et al.*, "All-fiber-optic VOC gas sensor based on side-polished fiber wavelength selectively coupled with cholesteric liquid crystal film," *Sensors and Actuators B: Chemical*, 2018, 273: 1816–1826.

[138] M. Khan, R. Rahaman, and S. W. Kang, "A high sensitivity and wide dynamic range fiber-optic sensor for low-concentration VOC gas detection," *Sensors*, 2014, 14(12): 23321–23336.

[139] Y. Xiao, J. Yu, L. Shun, S. Tan, X. Cai, Y. Luo, *et al.*, "Reduced graphene oxide for fiber-optic toluene gas sensing," *Optics Express*, 2016, 24(25): 28290–28302.

[140] H. Shan, C. Liu, L. Liu, J. Zhang, H. Li, Z. Liu, *et al.*, "Excellent toluene sensing properties of $SnO_2$-$F_{e2}O_3$ interconnected nanotubes," *ACS Applied Materials & Interfaces*, 2013, 5(13): 6376–6380.

[141] M. Parmar, C. Balamurugan, and D. W. Lee, "PANI and graphene/PANI nanocomposite films-comparative toluene gas sensing behavior," *Sensors*, 2013, 13(12): 16611–16624.

[142] I. Hafaiedh, W. Elleuch, P. Clement, E. Llobet, and A. Abdelghani, "Multi-walled carbon nanotubes for volatile organic compound detection," *Sensors and Actuators B: Chemical*, 2013, 182: 344–350.

[143] H. Zhang, Y. Chen, X. Feng, X. Xiong, S. Hu, Z. Jiang, *et al.*, "Long-range surface plasmon resonance sensor based on side-polished fiber for biosensing applications," *IEEE Journal of Selected Topics in Quantum Electronics*, 2018, 25(2): 1–9.

[144] J. Tang, Z. Li, M. Xie, Y. Zhang, W. Long, S. Long, *et al.*, "Optical fiber bio-sensor for phospholipase using liquid crystal," *Biosensors and Bioelectronics*, 2020, 170: 112547.

[145] N. Alberto, M. F. Domingues, C. Marques, P. André, and P. Antunes, "Optical fiber magnetic field sensors based on magnetic fluid: a review," *Sensors*, 2018, 18(12): 4325.

[146] Y. Chen, W. Sun, Y. Zhang, G. Liu, Y. Luo, J. Dong, *et al.*, "Magnetic nanoparticles functionalized few-mode-fiber-based plasmonic vector magnetometer," *Nanomaterials*, 2019, 9(5): 785.

[147] Y. Chen, Y. Hu, Y. Zhang, Z. Jiang, G. Liu, Y. Luo, *et al.*, "A portable smartphone-based vector-magnetometer illuminated and imaged via a side-polished-fiber functionalized with magnetic fluid," *IEEE Sensors Journal*, 2019, 20(3): 1283–1289.